# Autodetachment Dynamics of Acetaldehyde Enolate Anion, $CH_2CHO^-$

**Amy S. Mullin,† Kermit K. Murray,‡ C. P. Schulz,§ and W. C. Lineberger***

*Joint Institute for Laboratory Astrophysics, University of Colorado and National Institute of Standards and Technology and Department of Chemistry and Biochemistry, University of Colorado, Boulder, Colorado 80309-0440*

*Received: May 24, 1993®*

Autodetachment spectroscopy is used to investigate the dynamics of rotationally-induced electron detachment from the dipole-bound state of acetaldehyde enolate anion, $CH_2CHO^-$. Line width measurements for the deuterated enolate anion, $CD_2CDO^-$, provide information about the autodetachment mechanism. The observed line widths are compared to predictions of the rotationally adiabatic model developed by Clary. This comparison provides clues to the fundamental molecular interactions that govern autodetachment rates.

## I. Introduction

When a neutral molecule has a dipole moment of sufficient magnitude (~2 D), it is able to bind an extra electron in the dipolar field.[1-7] The resulting negative ion exists in a weakly bound state (5–100 $cm^{-1}$) with the extra electron in a diffuse orbital beyond the positive end of the dipole. The geometry of the dipole-bound anion is similar to that of the corresponding neutral molecule. These dipole-bound negative ion states are analogous to Rydberg states of neutrals, where the electron is weakly bound in a diffuse orbital and the nuclear geometry is very much like that of the cationic core. In a Rydberg state, the electron is bound by the $1/r$ Coulomb attraction to the positive core and an infinite number of Rydberg states exist for a given molecule. In molecular dipole-bound states, the electron is bound by the $(\cos\theta)/r^2$ charge-dipole potential, and for dipole moments of ~2–3 D, typically only one dipole-bound state exists. While theory predicts a larger number of dipole bound states for molecules having $\mu_D > 3$ D, there is as yet no experimental evidence for their existence. A somewhat analogous case occurs for H atoms where the near degeneracy between the *n*s and *n*p states is such that a distant electron can induce a "permanent" dipole moment, resulting in an effective $1/r^2$ long-range potential. Such excited anion states are seen as resonances in $H^-$ photodetachment.[8,9]

The existence of dipole-bound electrons was first suggested by low-energy electron scattering studies[10,11] on polar molecules which showed resonances near zero electron energy. The most direct experimental evidence has come from photoexcitation studies of anions in which the corresponding neutral can have a dipole-bound state. In these experiments, the valence ground state of the anion is photoexcited to the dipole-bound state, in which the electron is only bound by 5–100 $cm^{-1}$. With sufficient rotational and vibrational excitation in the dipole-bound state, it is possible for this state to autodetach via a rotation–electronic coupling mechanism. The experiments detect this photoabsorption process by the presence of sharp resonances in the near-threshold photodetachment cross section. The basic processes of photoexcitation and autodetachment are shown in Figure 1. Autodetachment resonances were first observed by Brauman and coworkers in photodetachment studies[12,13] of polar ions in an ion cyclotron resonance spectrometer. In these experiments, the photon energy resolution (~1 $cm^{-1}$) was not adequate to resolve rotational structure. Subsequent high-resolution (0.003 $cm^{-1}$) photodetachment studies using coaxial laser-ion beam methods have provided definitive evidence for dipole-bound states with the observation of rotationally resolved autodetachment resonances from short-lived dipole-bound states of $CH_2CHO^-$,[4] $CH_2CFO^-$,[5] $CH_2CN^-$,[7,14] $FeO^-$,[15] and $C_3H_2^-$.[16] Line width measurements for these resonances have demonstrated that there is a substantial rotational-state dependence in the autodetachment rates which arises from the structures and energies of the specific ion. In particular, for $FeO^-$ and $CH_2CN^-$, the autodetachment rate suddenly increases for states above a given rotational level. These rapid rate enhancements have been attributed to energetically favorable channel openings in the neutral product energy levels. If the rotationally-induced autodetachment is sufficiently rapid, then the characteristic signature of dipole bound states, sharp resonances in the near-threshold photodetachment cross section, is not observed. Brinkman et al.[17] have very recently proposed a simple model rationalizing this observation, suggesting that resonances will not be observed when the dipole moment vector has an orientation quite different from the principal moment axis. In the data reported here, the two vectors have sufficiently similar orientations that fairly sharp lines are observed for the lower rotational states. It is in this limit that we wish to compare the observed lifetimes with the predictions of theoretical models.

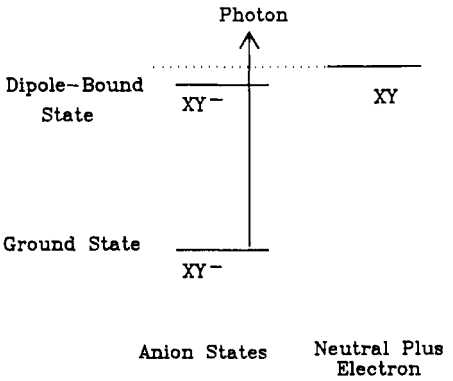


**Figure 1.** Photoexcitation from an anion valence state to an electronically-excited dipole-bound state can result in autodetachment of the electron when the rotational and vibrational levels in the dipole-bound state lie in the photodetachment continuum. The autodetachment process is observed as resonances in the photodetachment cross section.

Theoretically, the behavior of rotational–electronic autodetachment has been developed by Simons and co-workers[18,19] using a Golden Rule approach[20,21] to express the autodetachment rate

† Present address: Department of Chemistry, Columbia University, New York, NY 10027.
‡ Present address: Department of Chemistry, Texas A & M University, College Station, TX 77843.
§ Present address: Max Born Institute, Rudower Chaussee 6, O-1199 Berlin-Aldershof, Germany.
* To whom correspondence should be addressed.
® Abstract published in *Advance ACS Abstracts*, September 15, 1993.

0022-3654/93/2097-10281$04.00/0 

in a *product form* as

$$\text{rate} = (2\pi/\hbar)|\langle\psi_f^{rot}|\langle\psi_f^{elec}|T|\psi_i^{elec}\rangle|T\psi_i^{rot}\rangle|^2\rho$$

where $T$ is the rotational–electronic coupling operator, $\psi_i^{elec}$ and $\psi_i^{rot}$ are the electronic and rotational portions of the dipole-bound state anion wave function, $\psi_f^{elec}$ and $\psi_f^{rot}$ are the final-state (neutral plus electron) electronic and rotational wave functions, and $\rho$ is the density of final states. Autodetachment will occur more rapidly when there is favorable overlap of the initial and final wave functions and the coupling between the states is strong. In particular, the rotational–electronic coupling integral involves the electronic force operator and is expected to be large if a distortion of the molecular framework results in a deformation of the highest occupied molecular orbital in the anion.

Several important factors can influence[22] the autodetachment rate. The first of these is the energy difference between the anion rotational state and the neutral rotational state. As this energy difference is decreased, the probability for autodetachment increases. Additionally, autodetachment of the extra electron should be more facile when there is the smallest change in $J$, the total angular momentum, in going from the initial anion to the final neutral state. Thus, as the rotational manifolds of the initial and final states come more nearly into energy resonance and more favorable autodetachment channels become energetically accessible, the autodetachment rate will increase.[14]

The Golden Rule analysis has been used successfully to account for many autodetachment processes.[14,15,23] In an alternative approach, the autodetachment event is considered an electron–molecule half-collision, and scattering theory is used to describe the process. Recently, a physically simple model for autodetachment of dipole-bound states has been developed by Clary.[24] In this theory, the binding and subsequent ejection of an electron by the rotating polar molecule is described using rotationally adiabatic potentials. This rotationally adiabatic theory approximates a dipole-bound state as a rotating polarizable dipole with an "extra" electron. A rotationally adiabatic potential curve is derived which governs the electron motion and is used in electron scattering calculations to yield autodetachment line positions and widths. Clary's[24] numerical results were limited to the autodetachment dynamics of acetaldehyde enolate anion, $CH_2CHO^-$, and cyanomethyl anion, $CH_2CN^-$, where comparisons between experiment and theory are possible. Differences in molecular symmetry between $CH_2CHO^-$ and $CH_2CN^-$ are expected to result in distinct mechanisms for the electron detachment, and in addition, the resonance line widths for $CH_2CHO^-$ are predicted to exhibit substantial isotope effects. While previous studies[4] from this laboratory had addressed differences between $CD_2CDO^-$ and $CH_2CHO^-$ detachment processes, no information regarding line widths of the isotopically substituted enolate anion was available. We were thus prompted to extend the earlier high-resolution work to include measurement of the $CD_2CDO^-$ line widths, in order to test these aspects of the rotationally adiabatic model.

In this paper, the essential elements of Clary's rotationally adiabatic theory are explained as they relate to the autodetachment of acetaldehyde enolate anion. The autodetachment line widths for the deuterated enolate anion $CD_2CDO^-$ are presented, and resonance widths for $CH_2CHO^-$ and $CD_2CDO^-$ are compared with theoretical values. The autodetachment dynamics for the dipole-bound states of $CH_2CHO^-$ and $CD_2CDO^-$ are discussed in light of the theoretical predictions, and possible reasons for discrepancies between experiment and theory are presented.

## II. Rotationally Adiabatic Theory

In this model,[24] the neutral molecule is described as a rotating polarizable dipole. The dipole-bound electron is assumed to be completely separate from the electrons of the core neutral, and electron exchange and correlation are not taken explicitly into account. An effective potential between the electron and the neutral arises from interaction of the electron with the dipole and the charge-induced dipole. This effective potential is calculated for each value of the total angular momentum of the system, $J$, and is given in terms of the dipole moment $\mu_D$ and the polarizability $\alpha$ of the neutral as

$$V_J(R,\theta) = \left(\frac{-\alpha}{2R^4} + \frac{\mu_D \cos\theta}{R^2}\right) f(R)$$

where $R$ is the distance between the electron and the center of mass of the neutral and $\theta$ is the angle between the vector $R$ and the dipole. The damping function $f(R)$ vanishes at small $R$ to remove the unphysical nature of these potentials for small $R$. Interactions at small distances are not explicitly taken into account, which is reasonable since the dipole-bound electron is in a diffuse orbital that extends ~10–100 Å from the neutral core.

The Hamiltonian for the system is defined in terms of a prolate symmetric top with the dipole moment lying along the $a$-axis of the molecule, as in $CH_2CN^-$, and is given by

$$H = B\mathbf{j}^2 + (A-B)\mathbf{j}_z^2 + \frac{\mathbf{l}^2}{2R^2} + V(R,\theta)$$

where $A$ and $B$ are the rotational constants of the molecule, $\mathbf{j}^2$ is the rotational angular momentum operator for the molecule, $\mathbf{j}_z$ is the projection of $\mathbf{j}$ on the $a$-axis of the molecule and $\mathbf{l}^2$ is the orbital angular momentum operator for the electron. The eigenfunctions for the molecular rotation are the Wigner rotation functions, and the eigenfunctions for the electron orbital angular momentum are spherical harmonics. These are used as a basis for diagonalizing the Hamiltonian at fixed values of $R$, resulting in a set of adiabatic potential energy curves. For dipole moments up to 9 D, only one attractive curve is found[24] for each $J$ value, the total angular momentum (excluding spin), and each $k$ value, the projection of $J$ on the $a$-axis (corresponding to the $K_a$ quantum number). The attractive adiabatic potentials, labeled $\epsilon_{kJ}(R)$, are attractive at small $R$, have a centrifugal barrier (for $J \neq 0$) as $R$ increases, and tend to the rotationless neutral state as $R \to \infty$. As is discussed in section V, the nature of the potential at large $R$ is crucial for accurately describing an autodetachment event.

The adiabatic functions $\epsilon_{kJ}(R)$ are used in scattering calculations to locate resonances. These orbiting, or shape, resonances correspond to quasi-bound levels in the dipole-bound state with the electron trapped behind the barrier. Shape resonances with energies lying below the electron affinity of the anion are bound, and autodetachment is not energetically accessible; for resonances lying above the anion electron affinity, the electron can tunnel through the centrifugal barrier, resulting in autodetachment. Lifetimes for autodetachment are determined from the rate of barrier tunneling and are calculated to decrease as the total angular momentum of the electron–molecule system is increased. This is the result of two effects: (1) the energy of the resonance increases and is closer to the top of the centrifugal barrier, and (2) the barrier becomes narrower for higher $J$ states. The barrier is narrowed because all of the adiabatic potentials tend to the rotationless neutral state energy at large electron–molecule distances, which makes the large-$R$ slope of the high-$J$ barriers steeper than the low-$J$ barriers. Finally, for prolate symmetric tops with the dipole moment along the $a$-axis ($CH_2CN^-$), the tunneling lifetimes are predicted to depend only on $J$, and not on $k$.

The dipole moment of $CH_2CHO^-$ does not lie along a principal axis. Rather, it is pointed slightly off the $a$-axis and has a component along the $b$-axis. The $b$-axis component of the dipole moment acts to couple rotational states with the same total angular momentum $J$ but different $k$ values. This coupling is treated perturbatively in the rotationally adiabatic theory and permits the system to hop from one $k$ state to another, with $\Delta k = -1$. These hops between adiabatic curves correspond to the decay of

Feshbach resonances mentioned earlier and contribute to the line width of a resonance. For polar molecules with an off-axis dipole moment, such as $CH_2CHO^-$, Clary predicts an increase in the line width, varying as $(2K_a-1)^2$, as the $k$ state of the autodetaching level increases. In contrast, the $CH_2CN^-$ line widths are predicted to be insensitive to $k$. Additionally, the Feshbach contribution to the line width is predicted to have an $(A-B)^2$ dependence. The line widths for $CH_2CHO^-$ should be sensitive to isotopic substitution since, upon deuteration, the dipole moment will shift relative to the symmetry axes of the molecule and the rotational constants $A$ and $B$ will become smaller.

## III. Experimental Considerations

The photodetachment spectrometer used in this study has been described in detail previously.[4] A mass-selected ion beam is merged coaxially with the output of a single mode tunable ring dye laser, and the photodetachment spectrum is obtained by collecting the photodetached electrons as a function of photon energy and normalizing to laser power and ion current. Specifically, an ≈2-nA beam of $CD_2CDO^-$ is formed by extracting negative ions from a hot-cathode electric discharge that contains ≈0.4 Torr of a mixture of $d_6$-ethanol and CO. Ions with mass-to-charge ratio $m/q = 46$ are mass selected using a 90° magnet, accelerated to 2.2 keV, and merged coaxially with the laser beam in a 30-cm interaction region using electrostatic quadrupole deflectors. Detached electrons are collected by means of a weak magnetic field (~5 G) which guides the low-energy electrons into an electron multiplier. At the exit of the interaction region, the enolate ions and the neutral photodetachment products are separated by a second quadrupole deflector. The fast neutral beam passes through the deflector and impinges on a $CaF_2$ plate where secondary electrons are ejected and may be collected. The parent ion beam is deflected with the quadrupole into a Faraday cup, where the ion current is monitored.

A tunable home-built CW ring dye laser using DCM dye (610–680 nm) is operated single mode with 10-MHz resolution. Output powers of 250 mW are obtained when pumped with 5–6 W from all lines of an argon ion laser. Wavelength measurements to within 0.01 $cm^{-1}$ are made with a traveling Michelson interferometer. The overall resolution of the spectrometer is governed by the energy spread and angular divergence of the ion beam and the bandwidth of the laser. For these studies, the resolution is 40 MHz, primarily as a result of the initial energy spread in the ion source.

Laser frequency scanning and data collection are computer-controlled by scanning the laser and monitoring the electron count rate, laser power, and ion current simultaneously. For accurate line width measurements, the laser is locked to a scanning external cavity while the electron signal is collected. A fixed-distance etalon with a 250-MHz free spectral range is used to calibrate the frequency throughout a scan. The resonance line widths are measured by stepping the laser 10 MHz with a 2-s integration time per step. The strongest autodetachment resonances result in 30-kHz electron signal on top of a 10-kHz electron signal resulting from direct detachment. Scans are collected in 2.5-$cm^{-1}$ increments, normalized to laser power and ion current, and spliced together. The experimentally determined photon energy is Doppler corrected by ~5 $cm^{-1}$ to yield the photon energy absorbed by the fast ion beam.

## IV. $CD_2CDO^-$ Line Widths

The near-threshold photodetachment cross section of $CD_2CDO^-$ consists of a series of vibrational bands corresponding to transitions from the ground state of $CD_2CDO^-$ anions to autodetaching rotational levels in the dipole-bound state. High-resolution investigation of the (0,0) band reveals 45 resonances corresponding to autodetachment from 23 dipole-bound rotational levels. The line positions and assignments for this band have been determined previously.[4] The present study focuses on the measurement of resonance widths in order to elucidate details of the autodetachment dynamics. Before the experimental data are discussed, it is useful to consider the nature of autodetaching resonances.

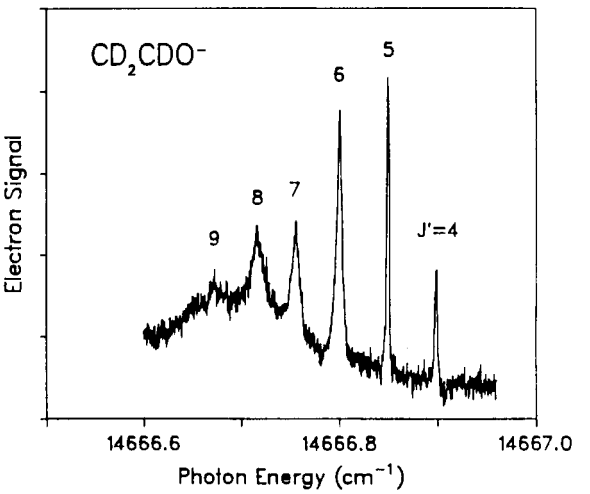


**Figure 2.** High-resolution scan of the $K_a = 1 \leftarrow K_a = 0$ Q-branch in $CD_2CDO^-$. The resonances are labeled with $J$ of the upper state and have line widths which correspond to autodetachment lifetimes.

Autodetachment line shapes are described by a Fano profile,[25]

$$\sigma(\epsilon) = \sigma_b + \frac{\sigma_a(\epsilon + q)^2}{\epsilon^2 + 1}$$

where $\sigma_b$ is the nonresonant contribution to the total cross section, $\sigma_a$ is the resonant contribution, and $\epsilon = (E - E_0)/(h\Gamma/2)$ is the reduced energy parameter and includes the energy $E$ and the fwhm, $\Gamma$, of the resonance. The square of the coupling parameter $q$ is a measure of the ratio of the autodetachment cross section to the direct detachment cross section. As $q \rightarrow \infty$, the autodetachment line shape becomes a symmetric Lorentzian with fwhm of $\Gamma$. For $CD_2CDO^-$, the cross sections for resonances are ~10–100 times greater than for direct detachment so the line shapes can be fit to a Lorentzian profile. The autodetachment lifetime $\tau$ in seconds is simply related to the spectral line width $\Gamma$ in hertz by the Heisenberg uncertainty principle and is given by $\tau = 1/2\pi\Gamma$. A line width of 0.01 $cm^{-1}$ (300 MHz) corresponds to an autodetachment lifetime of 500 ps. The peak intensity of the autodetachment signal is reduced for the very broad lines, and line width measurements are reported for resonances with $\Gamma$ up to ~1.5 GHz.

Acetaldehyde enolate anion is a near-prolate asymmetric top with rotational energy levels labeled by $J_{K_aK_c}$, where $J$ is the total angular momentum and $K_a$ and $K_c$ are the projections onto the principal axes of the molecule. Part of the autodetachment spectrum of $CD_2CDO^-$ is shown in Figure 2, where the resonances are labeled in $J$ and represent autodetachment from the $K_a = 1$, $K_c = J$ levels of the dipole-bound state. The line widths for autodetaching resonances of $CD_2CDO^-$ are presented in Table I. The narrowest lines have widths of 40–45 MHz, limited by the Doppler spread in the ion beam. Autodetachment from states with $K_a > 2$ is not observed for $CD_2CDO^-$ or $CH_2CHO^-$. The absence of these transitions is attributed to very short autodetachment lifetimes, resulting in resonances that are broadened beyond our ability to resolve from the smooth background.

The autodetachment resonances rapidly broaden with increasing rotational quantum number, as illustrated in Figure 2. This is observed for all $K_a$ states of $CH_2CHO^-$ and $CD_2CDO^-$. The resonance widths shown in Figure 2 correspond to autodetachment lifetimes that extend from ~200 ps to >4 ns in the space of four rotational quanta. Qualitatively, this rapid broadening of lines is a result of the weakly-bound electron decoupling from the dipole axis. As higher rotational states are excited, the overall

**TABLE I: Measured Resonance Widths[a] (fwhm) in MHz for Autodetaching $CD_2CDO^-$ Resonances[b]**

| $J$ | $J_{0\,J}$ | $J_{1\,J}$ | $J_{1\,J-1}$ | $J_{2\,J-2}$ | $J_{2\,J-1}$ |
|---|---|---|---|---|---|
| 0 | bound | bound | bound | bound | bound |
| 1 | bound | bound | bound | bound | bound |
| 2 | bound | bound | bound | <40 | 70 |
| 3 | bound | bound | bound | 200 | 250 |
| 4 | bound | <45 | <45 | 350 | 350 |
| 5 | <45 | 50 | 55 | 550 | 490 |
| 6 | 120 | 210 | 190 | ≥1500 | |
| 7 | 500 | 500 | 450 | | |
| 8 | 1100 | 750 | 750 | | |

[a] Uncertainties are ±20%. [b] The rotational quantum numbers of the autodetaching dipole-bound states are denoted by $J_{K_aK_c}$.

**TABLE II: Line Width Ratios for Different $K_a$ States of $CD_2CDO^-$ [a]**

| $J$ | $\Gamma(K_a=2)$ | $\Gamma(K_a=1)$ | $\Gamma(2)/\Gamma(1)$ |
|---|---|---|---|
| 4 | 350 | <45 | >7.8 |
| 5 | 550 | 55 | 10 |
| 6 | >1500 | 190 | >7.9 |
| $J$ | $\Gamma(K_a=1)$ | $\Gamma(K_a=0)$ | $\Gamma(1)/\Gamma(0)$ |
| 5 | 55 | <45 | >1.2 |
| 6 | 190 | 120 | 1.6 |
| 7 | 450 | 500 | 0.9 |
| 8 | 750 | 1100 | 0.7 |

[a] Line widths are in MHz. The rotationally adiabatic theory of Clary predicts $\Gamma(2)/\Gamma(1) \approx 9$ and $\Gamma(1)/\Gamma(0) \approx 1$.

molecular rotation causes greater decoupling. When molecular rotation goes into higher $K_a$ states, the decoupling occurs even more readily. Since the dipole moment and therefore the dipole-bound electron do not lie along the $a$-axis, increased rotational motion about this axis results in an enhanced autodetachment rate.

## V. Comparison between Experiment and Theory

In this section, the experimentally determined resonance widths for $CH_2CHO^-$ and $CD_2CDO^-$ are compared with the predictions made by the rotationally adiabatic theory. The experimental widths for both anions are shown in Figures 3 and 4, along with the line widths calculated by Clary.[24] At the most general level, the rotationally adiabatic theory is able to reproduce the overall $J$ dependence of the autodetachment line widths of $CH_2CHO^-$ and $CD_2CDO^-$ and is fairly accurate in calculating the absolute line widths, especially for the lower $J$ states. The calculated line widths display the correct $J$ dependence, i.e., increasing in width as $J$ increases. In terms of absolute widths, the maximum difference between the measured and the calculated line widths for $CD_2CDO^-$ is at most a factor of 10. The differences for $CH_2CHO^-$ are even smaller. For the $K_a = 0$, 1, and 2 states of both anions, however, the model overestimates the line widths for autodetachment from the high-$J$ levels.

For both $CH_2CHO^-$ and $CD_2CDO^-$, there is a strong $K_a$ dependence in the experimental line widths. The rotationally adiabatic theory predicts a $(2K_a-1)^2$ dependence for states with $K_a > 0$. The predicted factor of 9 between line widths of $K_a = 1$ and $K_a = 2$ states is in general agreement with our data. Note that, in Figures 3 and 4, the scale of the $y$-axes is over a factor of 2 different for the $K_a = 0$ and $K_a = 2$ states and there is a dramatic increase in the $K_a = 2$ resonance widths. This is summarized in Table II where the ratio of line widths for the $K_a$ states is shown. The $K_a = 2$ line widths are approximately 9 times greater than the $K_a = 1$ line widths, and there is almost no difference between the line widths for the $K_a = 0$ and $K_a = 1$

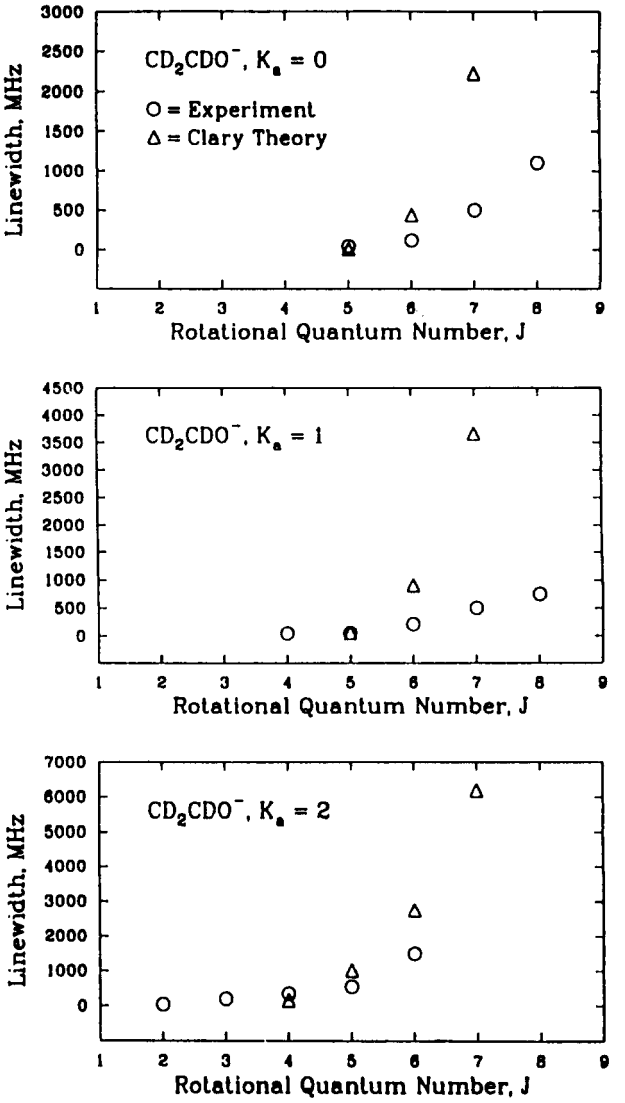


**Figure 3.** Observed and calculated autodetachment line widths of the different $K_a$ states of $CD_2CDO^-$. Note that $K_a = 2$ states have dramatically faster autodetachment rates than do the $K_a = 0$ states.

states. Similar behavior is present in $CH_2CHO^-$ which has autodetachment line widths for $J = 5$ of 100, 275, and 2900 MHz for the $K_a = 0$, $K_a = 1$, and $K_a = 2$ states, respectively.

Another prediction of the rotationally adiabatic theory is that, for $CH_2CHO^-$ states where a Feshbach mechanism is possible (states with $K_a > 0$ which can curve hop), autodetachment rates should increase upon isotopic substitution with an $(A - B)^2$ dependence. Using the Mead et al.[4] values for $A$ and $B$, we find the ratio of $CH_2CHO^-$ line widths to $CD_2CDO^-$ line widths is predicted to be 2.79. In Table III, the line widths for the different $K_a$ states of both anions are shown along with the ratio of the line widths. For $K_a = 1$, the experimental ratio is in good agreement with theory. The $K_a = 2$ states with $J = 3$–5 are a factor of 2–3 higher than predicted. The experimental ratio of >27.5 for $J = 2$ is consistent with the rotationally adiabatic model, which indicates that the $J = 2$, $K_a = 2$ state in $CD_2CDO^-$ is bound. Although not predicted to have an isotope dependence, the line widths for the $K_a = 0$ states are 2–3 times narrower for $CD_2CDO^-$ than for $CH_2CHO^-$. This suggests that additional mechanisms may be important for autodetachment of the $K_a = 0$ states.

The rotationally adiabatic theory is a powerful method for predicting resonance widths in autodetachment spectra of dipole-bound states. Many of the observed trends are calculated with the theory. Discrepancies between the observed line widths and those calculated with Clary's method can be attributed to details of the electron-dipole potential which are neglected in the adiabatic

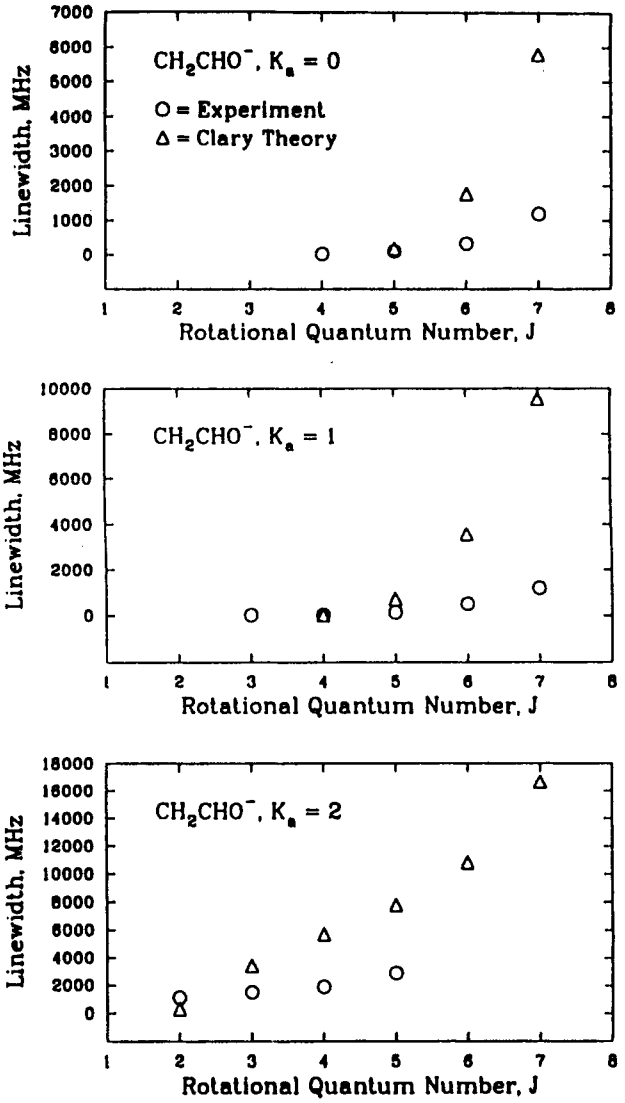


**Figure 4.** Observed and calculated autodetachment line widths of the different $K_a$ states of $CH_2CHO^-$. Note that, like the deuterated line widths in Figure 3, the $K_a = 2$ states have much faster autodetachment rates than do the $K_a = 0$ states.

**TABLE III: Comparison of Measured Autodetaching Line Widths Γ for $CH_2CHO^-$ and $CD_2CDO^-$ [a]**

| $J$ | $\Gamma(CH_2CHO^-)$ | $\Gamma(CD_2CDO^-)$ | $\Gamma(H)/\Gamma(D)$ |
|---|---|---|---|
| | | $K_a = 0$ | |
| 5 | 100 | <45 | >2.2 |
| 6 | 330 | 120 | 2.8 |
| 7 | 1200 | 500 | 2.4 |
| | | $K_a = 1$ | |
| 4 | 25 | <45 | >0.5 |
| 5 | 140 | 50 | 2.8 |
| 6 | 510 | 210 | 2.4 |
| 7 | 1200 | 500 | 2.4 |
| | | $K_a = 2$ | |
| 2 | 1100 | <40 | >27.5 |
| 3 | 1500 | 200 | 7.5 |
| 4 | 1900 | 350 | 5.4 |
| 5 | 2900 | 550 | 5.3 |

[a] Line widths are given in MHz. The ratio of the line widths of $CH_2CHO^-$ to those for $CD_2CDO^-$ is predicted by the rotationally adiabatic theory to have a value of 2.79. Data for $CH_2CHO^-$ are from ref 4.

approximation. In particular, the adiabatic potentials are defined for a total angular momentum $J$ and are a composite of all possible final rotational levels of the neutral and angular momentum states of the electron. As the electron detaches, it is described as moving along this adiabatic curve which inevitably results in a rotationless neutral and an electron with many quanta of orbital angular momentum. In reality, the system is not necessarily moving along one adiabatic curve as the detachment occurs; rather, it may undergo a series of curve crossings that will enhance or diminish the autodetachment rates accordingly.

In a modified rotationally adiabatic theory, Simons[26] has suggested that, by taking these final-state curve crossings into account, the precise details of the autodetachment process can be recovered. In his elaboration, Simons calculates the curve crossing probabilities for the final rotational states and uses them to adjust the line widths obtained by Clary. This procedure has been applied[26] to the autodetachment line widths of $CH_2CN^-$ and has been more successful in accurately reproducing some of the finer details of the line width behavior. While it has not yet been applied to the more complex $CH_2CHO^-$ case, the increased physical content inherent in the modified rotationally adiabatic model promises better insight into the physical nature of the rotation–electronic autodetachment process. What is really needed is an experiment capable of determining the final rotational quantum state of the neutral molecular product. At present, such an experiment appears prohibitively difficult.

## VI. Conclusions

The resonance widths for autodetachment from the dipole-bound state of $CD_2CDO^-$ are reported and compared with recent theoretical results. The observed line widths show substantial variation with the total angular momentum $J$ and with $K_a$, the projection of $J$ on the $a$-axis of the anion. The theory proposed by Clary[24] is a physically simple model that represents the interaction of the departing electron and the polar neutral with an adiabatic potential. In this theory, the dipole-bound state of the anion is described by a rotating polarizable dipole interacting with an electron. The adiabatic potentials are used in scattering calculations to find resonance positions and widths. There is substantial agreement between the observed and calculated line widths; the rotationally adiabatic theory reproduces the overall $J$ dependence for autodetaching line widths as well as trends between different $K_a$ states and effects resulting from isotopic substitution. Discrepancies in the absolute magnitude of some of the linewidths may be a result of modeling a complex, multidimensional process by a simple adiabatic potential. In spite of this, the rotationally adiabatic theory is a powerful and useful tool for predicting the occurrence of diple-bound resonances and approximating the autodetachment line widths. With modifications[26] to include final-state effects, the rotationally adiabatic theory has been successful in reproducing some of the finer details of experimental line widths for $CH_2CN^-$, indicating that final-state coupling is important in determining autodetachment line widths.

**Acknowledgment.** We thank Professors David Clary and Jack Simons for many helpful discussions on the details of autodetaching states and for their extensive theoretical efforts. This work was funded by NSF Grants CHE88-19444 and PHY90-12244.

## References and Notes

(1) Fermi, E.; Teller, E. *Phys. Rev.* **1947**, *72*, 406.
(2) Garrett, W. R. *Chem. Phys. Lett.* **1970**, *5*, 393. Garrett, W. R. *Phys. Rev. A* **1971**, *3*, 961.
(3) Lykke, K. R.; Mead, R. D.; Lineberger, W. C. *Phys. Rev. Lett.* **1984**, *52*, 2221.
(4) Mead, R. D.; Lykke, K. R.; Lineberger, W. C.; Marks, J.; Brauman, J. I. *J. Chem. Phys.* **1984**, *81*, 4883.
(5) Marks, J.; Brauman, J. I.; Mead, R. D.; Lykke, K. R.; Lineberger, W. C. *J. Chem. Phys.* **1988**, *88*, 6785.
(6) Andersen, T.; Lykke, K. R.; Neumark, D. M.; Lineberger, W. C. *J. Chem. Phys.* **1987**, *86*, 1858.

(7) Lykke, K. R.; Neumark, D. M.; Andersen, T.; Trapa, V. J.; Lineberger, W. C. *J. Chem. Phys.* **1987**, *87*, 6842.
(8) Harris, P. G.; Bryant, H. C.; Mohagheghi, A. H.; Reeder, R. A.; Sharifian, H.; Tang, C. Y.; Tootoonchi, H.; Donahue, J. B.; Quick, C. R.; Rislove, D. C.; Smith, W. W.; Stewart, J. E. *Phys. Rev. Lett.* **1990**, *65*, 309.
(9) Sadeghpour, H. R.; Greene, C. H. *Phys. Rev. Lett.* **1990**, *65*, 313.
(10) Wong, S. F.; Schulz, G. J. *Phys. Rev. Lett.* **1974**, *33*, 134.
(11) Rohr, K.; Linder, F. *J. Phys. B* **1976**, *9*, 2521.
(12) Zimmerman, A. H.; Brauman, J. I. *J. Chem. Phys.* **1977**, *66*, 5823. Jackson, R. J.; Zimmerman, A. H.; Brauman, J. I. *J. Chem. Phys.* **1979**, *71*, 2088.
(13) Jackson, R. L.; Hiberty, P. C.; Brauman, J. I. *J. Chem. Phys.* **1981**, *74*, 3705.
(14) Marks, J.; Wetzel, D. M.; Comita, P. B.; Brauman, J. I. *J. Chem. Phys.* **1986**, *84*, 5284.
(15) Andersen, T.; Lykke, K. R.; Neumark, D. M.; Lineberger, W. C. *J. Chem. Phys.* **1987**, *86*, 1858.
(16) Yokayama, K.; Kim, J.; Leach, G. R.; Lineberger, W. C. *J. Chem. Phys.*, in press.
(17) Brinkman, E. A.; Berger, S.; Marks, J.; Brauman, J. I. *J. Chem. Phys.*, submitted.
(18) Simons, J. *J. Am. Chem. Soc.* **1981**, *103*, 3971.
(19) Chalasinski, G.; Kendall, R. A.; Taylor, H.; Simons, J. *J. Phys. Chem.* **1988**, *92*, 3086.
(20) Wentzel, G. *Z. Phys.* **1926**, *40*, 574; **1927**, *41*, 828.
(21) Berry, R. S. *J. Chem. Phys.* **1966**, *45*, 1228.
(22) Berry, R. S. *Adv. Electron. Electron Phys.* **1980**, *51*, 137. Berry, R. S.; Leach, S. *Adv. Electron. Electron Phys.* **1981**, *57*, 1.
(23) Hefter, U.; Mead, R. D.; Schulz, P. A.; Lineberger, W. C. *Phys. Rev. A* **1983**, *28*, 1429.
(24) Clary, D. C. *J. Phys. Chem.* **1988**, *92*, 3173.
(25) Fano, U. *Phys. Rev.* **1961**, *124*, 1866.
(26) Simons, J. *J. Chem. Phys.* **1989**, *91*, 6858.